Biochimica et Biophysica Acta 1850 (2015) 784–793

Contents lists available at ScienceDirect

Biochimica et Biophysica Acta

journal homepage: www.elsevier.com/locate/bbagen

Activation of muscarinic receptors in rat parotid acinar cells induces AQP5 trafficking to nuclei and apical plasma membrane

Gota Cho [a], Aneta M. Bragiel [b], Di Wang [b], Tomasz D. Pieczonka [b], Mariusz T. Skowronski [c], Masayuki Shono [d], Søren Nielsen [c], Yasuko Ishikawa [b,*]

[a] Department of Dental Anesthesiology, Institute of Health Biosciences, The University of Tokushima Graduate School, 3-18-15 Kuramoto-cho, Tokushima 770-8504, Japan
[b] Department of Medical Pharmacology, Institute of Health Biosciences, The University of Tokushima Graduate School, 3-18-15 Kuramoto-cho, Tokushima 770-8504, Japan
[c] Institute of Medicine and Health Technology, Aalborg University, DK-9220 Aalborg, Denmark
[d] Support Center for Advanced Medical Sciences, Institute of Health Biosciences, The University of Tokushima Graduate School, 3-18-15 Kuramoto-cho, Tokushima 770-8504, Japan

ARTICLE INFO

Article history:
Received 8 August 2014
Received in revised form 24 December 2014
Accepted 12 January 2015
Available online 17 January 2015

Keywords:
Aquaporin-5
Trafficking
Nuclei
Apical plasma membrane
Parotid glands
Acinar cells

ABSTRACT

Background: The subcellular distribution of aquaporin-5 (AQP5) in rat parotid acinar cells in response to muscarinic acetylcholine receptor (mAChR) activation remains unclear.
Methods: Immunoconfocal and immunoelectron microscopy were used to visualize the distribution of AQP5 in parotid acinar cells. Western blotting was used to analyze AQP5 levels in membranes. To clarify the characteristics of membrane domains associated with AQP5, detergent solubility and sucrose-density flotation experiments were performed.
Results: Under control conditions, AQP5 was diffusely distributed on the apical plasma membrane (APM) and apical plasmalemmal region and throughout the cytoplasm. Upon mAChR activation, AQP5 was predominantly located in the nucleus, APM and lateral plasma membrane (LPM). Subsequently, localization of AQP5 in the nucleus, APM and LPM was decreased. Prolonged atropine treatment inhibited mAChR agonist-induced translocation of AQP5 to the nucleus, APM and LPM. AQP5 levels were enhanced in isolated nuclei and nuclear membranes prepared from parotid tissues incubated with mAChR agonist. mAChR agonist induced AQP5 levels in both soluble and insoluble nuclear fractions solubilized with Triton X-100 or Lubrol WX. Small amounts of AQP5 in nuclei were detected using low-density sucrose gradient. When AQP5 was present in the nuclear membrane, nuclear size decreased.
Conclusion: The activation of mAChR induced AQP5 translocation to the nucleus, APM and LPM, and AQP5 may trigger water transport across the nuclear membrane and plasma membrane in rat parotid acinar cells.
General significance: AQP5 translocates to the nuclear membrane and may trigger the movement of water, inducing shrinkage of the nucleus and the start of nuclear functions.

1. Introduction

Parotid glands are innervated by both sympathetic and parasympathetic nerves. The activation of M_3- and M_1-muscarinic acetylcholine receptors (mAChRs) and α_1-adrenoceptors increases intracellular calcium concentrations ($[Ca^{2+}]i$) and induces salivary fluid secretion [1,2]. Aquaporins (AQPs) are a family of integral membrane proteins that exhibit specific channel activity for water. To date, 13 AQPs have been cloned and classified into 3 major subtypes; classical aquaporins (AQP0, −1, −2, −4 and −5), aquaglyceroporins (AQP3, −7, −9 and −10), and unorthodox aquaporins (AQP6, −8, −11 and −12) [3,4]. Salivary fluid secretion is defective in transgenic mice lacking AQP5 [5], indicating a crucial role for AQP5 in salivary fluid secretion [6].

In vitro experiments using rat parotid gland slices demonstrated that acetylcholine (ACh) and epinephrine acting at M_3- and M_1-mAChRs and α_1-adrenoceptors, respectively, induce a rapid increase in AQP5 in the apical plasma membrane (APM) by increasing intracellular Ca^{2+} concentration $[Ca^{2+}]i$ [7,8]. The muscarinic agonist cevimeline, acting at M_3- and M_1-mAChRs, induces long-term increases in AQP5 levels in the APM [9]. In vivo experiments using confocal microscopy revealed that in the parotid gland under unstimulated conditions, AQP5 is located in lipid rafts that contain flotillins and prototypical ganglioside GM1 with a diffuse pattern in apical cytoplasm in duct cells. The activation of M_3- and M_1-mAChRs induces the rapid translocation of AQP5, together with lipid rafts, from the apical cytoplasm to the APM by enhancement of $[Ca^{2+}]i$ [10,11]. AQP5 and lipid rafts are then released into saliva [12]. AQP5 is known to be present in parotid gland exosomes [13,14], which accumulate within multivesicular bodies and are released into saliva from parotid cells upon fusion of multivesicular bodies with the plasma membrane in a Ca^{2+}-triggered reaction [15,16]. In salivary glands, the Ca^{2+}-permeable transient receptor potential

* Corresponding author at: Department of Medical Pharmacology, Tokushima University Graduate School, 3-18-15 Kuramoto-cho, Tokushima 770-8504, Japan. Tel./fax: +81 88 633 7332.
E-mail address: yisikawa@tokushima-u.ac.jp (Y. Ishikawa).

http://dx.doi.org/10.1016/j.bbagen.2015.01.009
0304-4165/

canonical 1 (TRPC1) plays an important role in the agonist-induced increase in $[Ca^{2+}]i$ [2,17]. AQP5 was also demonstrated to be rapidly translocated from the cytoplasm to the APM by enhancement of $[Ca^{2+}]i$ during sweating in sweat glands [18].

Salivary glands consist of three major types (parotid, submandibular and sublingual glands) and numerous minor glands. The submandibular, sublingual, and minor salivary glands are continuously active, whereas the parotid glands have no measurable unstimulated secretion, but become the main source of saliva when stimulated [19,20]. Primary saliva is formed in acinar cells [1] and AQP5 shows rapid translocation to the APM upon activation of M_3-muscarinic receptors. Therefore, the first aim in the present study was to directly visualize the detailed time-dependent AQP5 translocation in the parotid acinar cells stimulated by cevimeline.

Lipid rafts are membrane microdomains enriched with cholesterol and glycosphingolipids [21,22], and are implicated in the regulation of membrane trafficking [23–25], clustering of membrane-associated proteins [26] and intracellular signaling [27,28]. Raft components are insoluble in Triton X-100 (TX-100) and float to low density in sucrose density gradients [27,29]. Rafts are characterized by differences in detergent insolubility. Rafts in the direct pathway from the trans-Golgi network to the APM are soluble in TX-100 and insoluble in Lubrol, whereas rafts in the indirect pathway are both Lubrol and TX-100 insoluble [30,31]. AQP5 that is translocated to the APM is distributed in TX-100- and Lubrol-insoluble rafts [10].

In this study, we found that upon activation of mAChRs, AQP5 is trafficked to the nuclear membrane and APM. The second aim of this study was to clarify the vesicle type associated with AQP5 trafficking to nuclei. The third aim of this study was to investigate the function of AQP5 in the nuclear membrane.

2. Materials and methods

2.1. Animals

Eight-week-old male Wistar rats were given standard laboratory chow (MF; Oriental Yeast, Tokyo, Japan) and water ad libitum, and were maintained in accordance with the guidelines established by the Animal Care Committee of the University of Tokushima Graduate School.

2.2. Immunohistochemistry

Cevimeline (5.0 mg/kg) was injected into the tail vein. At the indicated times after injection, parotid glands were quickly removed, embedded in Jung tissue freezing medium (Leica, Heidelberg, Germany), and rapidly frozen with liquid nitrogen. In some experiments, cevimeline was injected 60 min after intraperitoneal injection of atropine (200 mg/kg). Frozen sections (7 μm) were cut, mounted on poly-L-lysine-coated glass slides, and immediately fixed for 30 min with pre-chilled (−20 °C) ethanol. Immunostaining was performed as described previously [10]. After washing in phosphate buffered saline (PBS, pH 7.5), sections were blocked in avidin and biotin solutions (Zymed Laboratories Inc., South San Francisco, CA), followed by 1% membrane blocking agent (Amersham Biosciences, Buckinghamshire, UK) for 1 h, and were double-stained as follows. Sections were incubated at 4 °C overnight with primary antibodies; rabbit anti-AQP5 antibody (1:1000 dilution) and goat anti-flotillin-1 antibody (1:1000 dilution; Santa Cruz Biotechnology, Santa Cruz, CA), or rabbit anti-ganglioside GM1 antibody (1:1000 dilution; Calbiochem-Novabiochem Co., Darmstadt, Germany). This was followed by incubation for 1 h with biotinylated goat anti-rabbit antibody or horse anti-goat IgG antibody (Vector Laboratories, Burlingame, CA). These antibodies were raised against the COOH-terminal amino acid sequence of rat AQP5 and rabbit anti-AQP5 antibody was generated in response to a synthetic peptide (KGTYEPEEDWEDHREERKKTI) [5]. Labeling was visualized with streptavidin-conjugated Alexa Fluor 488 or Alexa Fluor 568 (1:1000 dilution; Molecular Probes, Inc., Leiden, Netherlands). To stain cell nuclei, sections were incubated with 0.5 μg/ml RNaseA, and then with 50 μg/ml of propidium iodide for 1 h at 37 °C. Fluorescence images were captured using a confocal microscope (TCS NT; Leica). Fluorescence images of sections excited at 488 or 568 nm, and excited simultaneously at both wavelengths, were captured using confocal laser scanning microscopy (Leica TCS NT) equipped with an Ar/Kr laser and a 40× dry objective (Leica Plan Apochromat). In some experiments, the nuclear diameter was measured using a microscopy ruler.

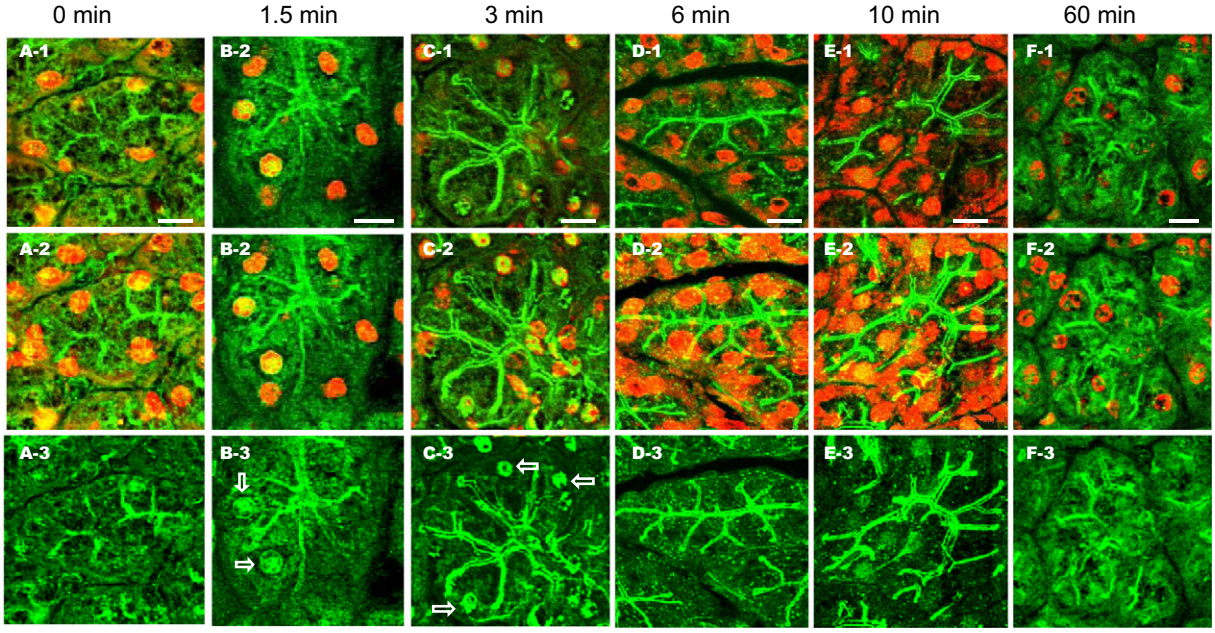

Fig. 1. Changes in AQP5 immunofluorescence in parotid acinar cells from cevimeline-injected rat. Parotid glands were obtained from rats at 0 (A), 1.5 (B), 3 (C), 6 (D), 10 (E) and 60 (F) min after cevimeline injection. Sections were fixed and incubated with anti-AQP5 antibody. Alexa-488 was used to visualize AQP5. Nuclei were stained with propidium iodide. One section is shown in each single image (−1). Sixteen consecutive images obtained with a confocal microscope were projected to generate a single image (−2). To facilitate visualization of AQP5 localization in nuclei, the 568 nm laser was turned off (−3). Arrow indicates AQP5 in the nuclei. Bars: 10 μm.

2.3. Isolation of nuclei and preparation of nuclear membrane

Glands were rapidly removed 3 min after saline or cevimeline injection, and were pooled in ice-cold SMD solution containing 0.32 M sucrose, 3 mM $MgCl_2$ and 1 mM dithiothreitol (DTT). All subsequent manipulations were carried out at 4 °C. Glands were sliced at 4 mm using a McIlwain Tissue Chopper (Mickel Laboratory Engineering Co., Surrey, UK) and were then homogenized in 5 volumes of SMD solution, using a glass homogenizer fitted with a loose Teflon pestle rotating at 1250 rpm for 12 strokes. Homogenates were filtered through nylon bolting cloth (110 mesh), and were centrifuged at 600 ×*g* for 10 min. The crude nuclear pellet was washed twice in SMD solution and finally

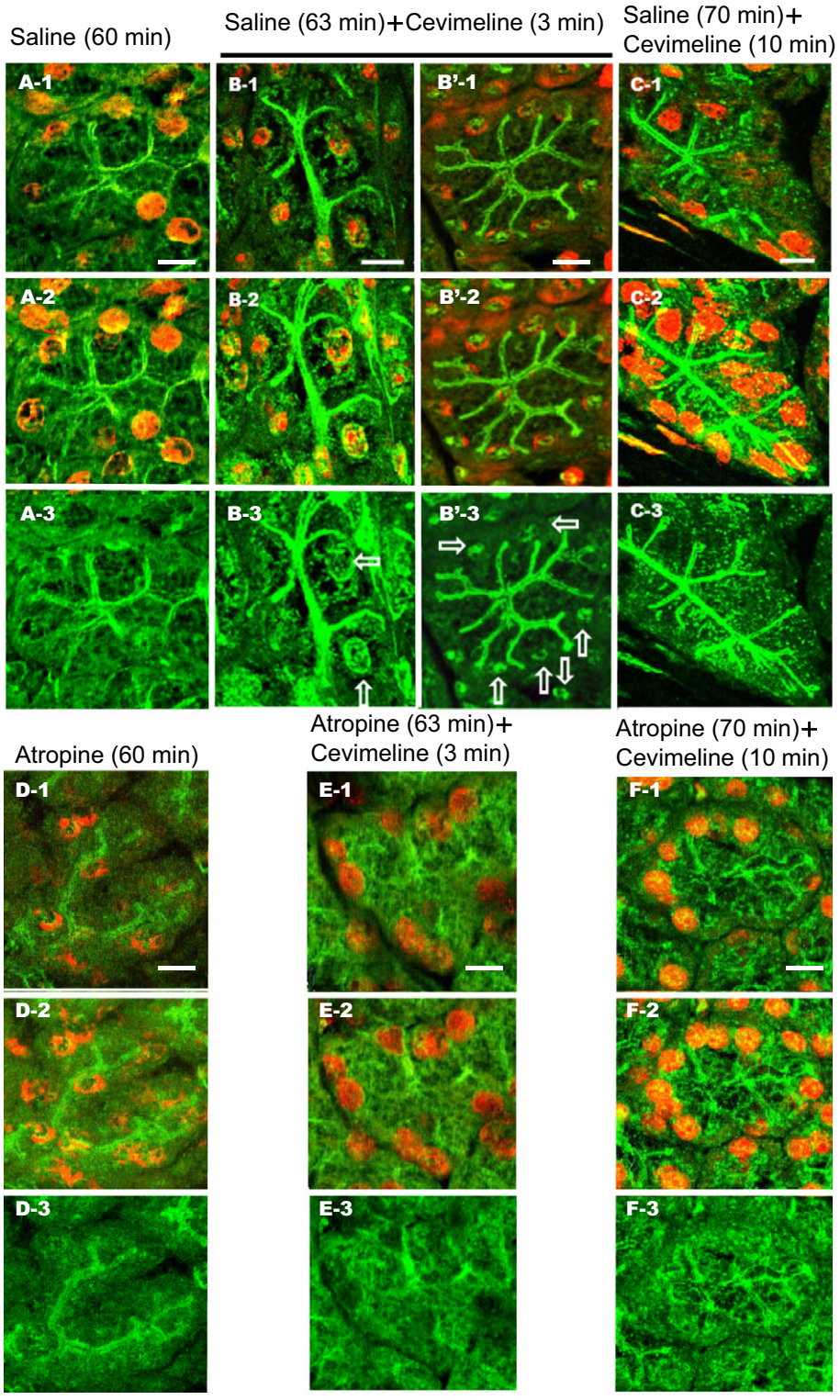

Fig. 2. Changes in AQP5 immunofluorescence in parotid acinar cells from atropine-injected rats. Rats were intraperitoneally injected with atropine (D–F) or saline (A–C). After 60 min, cevimeline was intravenously injected. Parotid glands were obtained from rats at 0 (A and D), 3 (B, B′, and E) and 10 (C and F) min after cevimeline injection. Alexa-488 and propidium iodide were used to visualize AQP5 and nuclei, respectively. One section is shown in each single image (−1). Sixteen consecutive images obtained with a confocal microscope were projected to generate a single image (−2). To facilitate visualization of AQP5 localization in nuclei, the 568 nm laser was turned off (−3). Arrow indicates AQP5 in the nuclei. Bars: 10 μm.

suspended in 3 ml of SMD solution. Nuclei were isolated using discontinuous sucrose-density gradients, as described previously [32]. Briefly, a suitable volume of 2.2 M sucrose solution containing 3 mM $MgCl_2$ and 1 mM DTT was added to this suspension to give a final sucrose molarity of 1.89. After mixing thoroughly, the suspension was layered over 2.2 M sucrose solution containing 3 mM $MgCl_2$ and 1 mM DTT, and was centrifuged at 75,000 ×*g* for 90 min using an RPS50 rotor (Hitachi Koki Co., Ltd., Tokyo, Japan).

Nuclear membranes were obtained as described previously [33]. Isolated nuclei were lysed in 8 mM Tris–HCl (pH 8.5) containing 0.1 mM $MgCl_2$, 4 mM 2-mercaptoethanol, 8% sucrose, and 1 μg/ml DNase I. After 10 min of incubation at 22 °C, the reaction was stopped by diluting lysates with cold water (1:1, vol/vol). Lysed nuclei were centrifuged at 38,000 ×*g* for 15 min at 4 °C, and the sediment was resuspended in 10 mM Tris–HCl (pH 7.4, containing 0.1 mM $MgCl_2$, 5 mM 2-mercaptoethanol, 10% sucrose and 1 μg/ml DNase I). Digestion was carried out for 20 min and was terminated by the addition of an equal volume of ice-cold distilled water. The final nuclear envelope pellet was obtained after centrifugation at 38,000 ×*g* for 15 min at 4 °C.

2.4. Preparation and incubation of rat parotid tissues

Parotid glands were rapidly removed from rats, and were then transferred into an ice-cold Krebs-Ringer Tris (KRT) solution (120 mM NaCl, 4.8 mM KCl, 1.2 mM KH_2PO_4, 1.2 mM $MgSO_4$, 1.0 mM $CaCl_2$, 16 mM Tris–HCl [pH 7.4], 5 mM glucose) aerated with O_2 gas. Tissue slices (0.4 mm) were prepared from the parotid glands using a McIlwain Tissue Chopper (Mickle Laboratory Engineering, Surrey, UK), and were equilibrated with KRT solution for 20 min at 37 °C with shaking, as described previously [7]. Slices (wet weight, 300 mg) were then incubated at 37 °C in 10 ml of KRT solution in the presence or absence of cevimeline.

2.5. Preparation of inner and outer nuclear membrane

In accordance with the method of Gilchrist and Pierce [34], nuclear membranes prepared from parotid tissues incubated with or without cevimeline were diluted to 2 mg/ml in SMD containing 1% citric acid (trisodium dehydrate) and incubated on ice for 15 min. The fraction containing inner nuclear membranes was pelleted at 5000 ×*g* for 10 min. The supernatant fraction containing the outer nuclear membrane was precipitated with 10% trichloroacetic acid.

2.6. Ganglioside extraction

Nuclei were homogenized with lysis buffer and extracted twice with chloroform/methanol/water (4:8:3 v/v/v), as described previously [35]. Upper layers were pooled, and distilled water was added to produce a final chloroform/methanol/water ratio of 1:2:1.4, followed by centrifugation for 30 min at 1500 ×*g*. The upper phase was collected. Methanol (half of lower phase volume) and 0.01 M KCl (20% of total volume of lower phase, plus added methanol) were added to the lower phase, followed by vortexing and centrifugation for 30 min at 2000 ×*g*. The two upper phases were combined and evaporated to dryness. The dried residue was dissolved in 2 ml 0.1 M KCl and recycled three times on a Sepak C18 column (1 ml). Bound material was eluted with methanol and chloroform/methanol (2:1).

2.7. Preparation of non-ionic detergent-insoluble and -soluble domains and gradient density flotation assay

Isolated nuclei were solubilized with TNE solution (25 mM Tris–HCl [pH 7.4], 150 mM NaCl, 5 mM EDTA) containing 1% TX-100 or 1% Lubrol WX on ice for 30 min. Soluble and insoluble fractions were then obtained by centrifugation at 200,000 ×*g* for 30 min at 4 °C. Nuclear membranes were solubilized with TNE solution containing 1% Triton X-100 and protease inhibitors [10] for 30 min, which was then brought up to 45% sucrose (w/v) in a final volume of 1 ml, and sequentially overlaid with 1.5 ml of 45%, 35% and 5% sucrose. Gradients were centrifuged at 240,000 ×*g* for 18 h. Six fractions (0.75 ml) were collected from the top (F1) to the bottom (F6) of the gradient. The pellet was designated as F7.

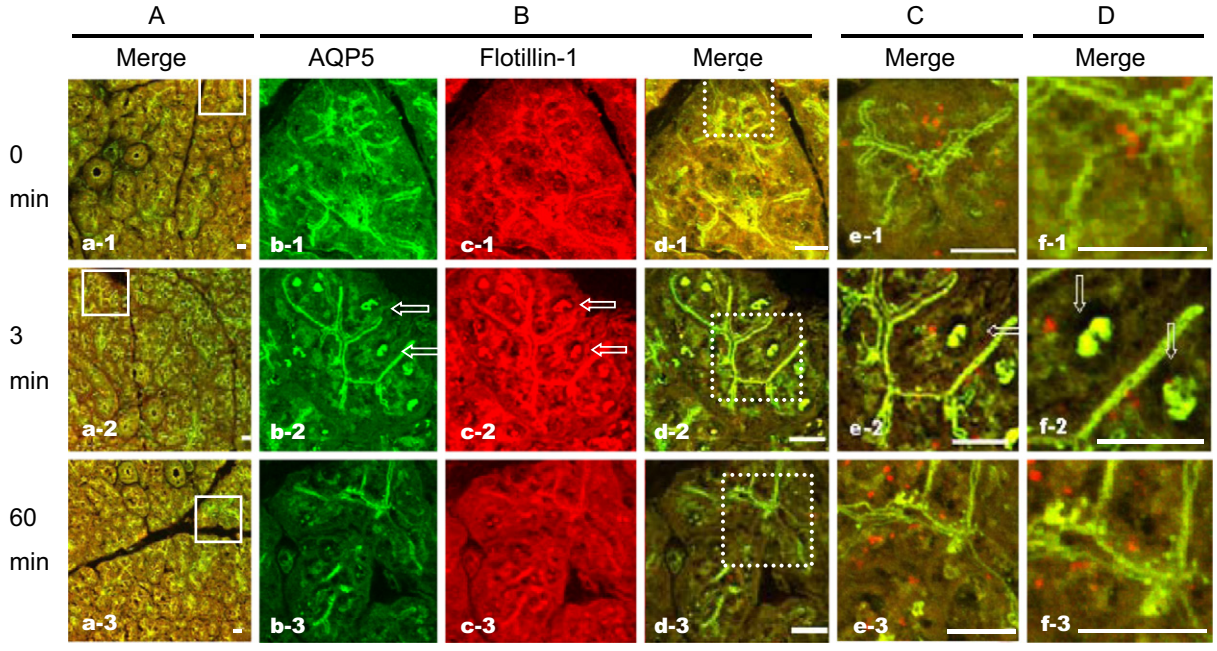

Fig. 3. Changes in immunofluorescence of AQP5 and flotillin-1 in parotid acinar cells from cevimeline-injected rats. Parotid glands from rats at 0 (a-1–f-1), 3 (a-2–f-2) and 60 (a-3–f-3) min after cevimeline-injection were fixed and then incubated with anti-AQP5 and anti-flotillin-1 antibodies. Alexa-488 and -568 were used to visualize AQP5 and flotillin-1, respectively. Magnification was increased to obtain photographs from A to D. White and transparent arrows indicate intracellular vesicles and AQP5 in the nuclei, respectively. Arrow indicates AQP5 in the nuclei. Bars: 10 μm.

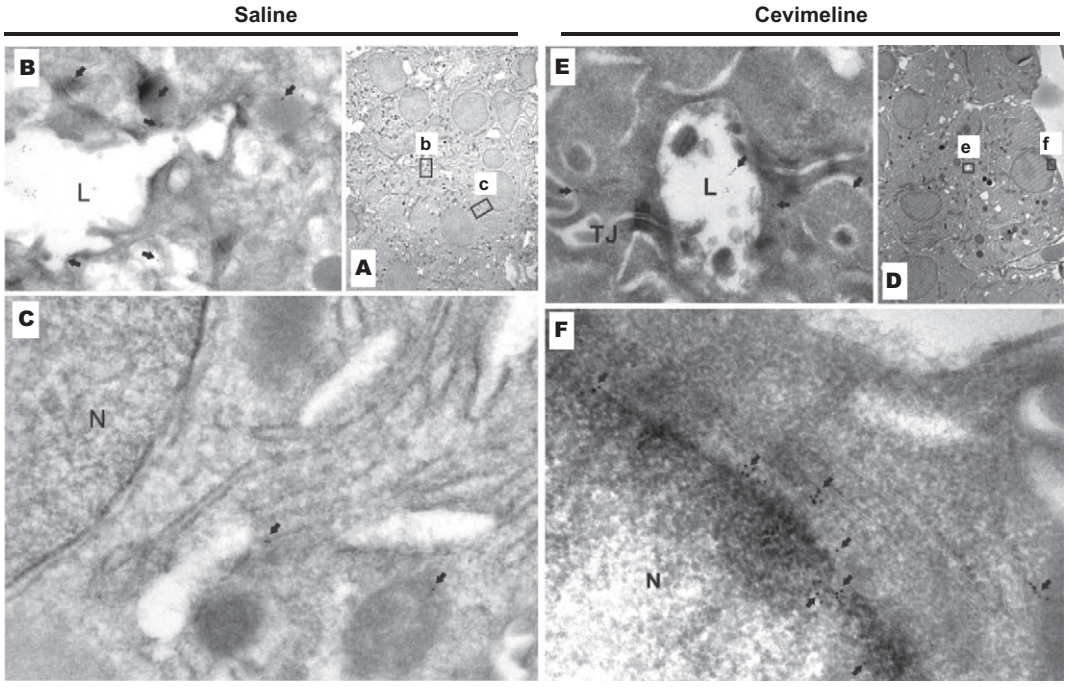

Fig. 4. Immunoelectron microscopy of AQP5 expression in acinar cells of rat parotid glands. A–C) Glands were removed from rats at 3 min after saline injection. Frames b and c are magnified in (B) and (C), respectively. Labeling is mainly observed at the intracellular components (arrows). Labeling is also observed in the intercellular canaliculi (arrows). L, Lumen of intercellular canaliculi; N, nucleus. Magnification: A, ×2000; B and C, ×16,000. D–F) Glands were removed from rats at 3 min after cevimeline injection. Frames e and f are magnified in (E) and (F), respectively. When compared with control tissues (Fig. 4A), changes are observed in subcellular localization of AQP5. Labeling is mainly associated with the nuclear membrane (arrows). Labeling is also observed in the lumen and intercellular canaliculi (arrows). L, lumen; N, nucleus; TJ, tight junction. Magnification: D, ×2000; E and F, ×16,000.

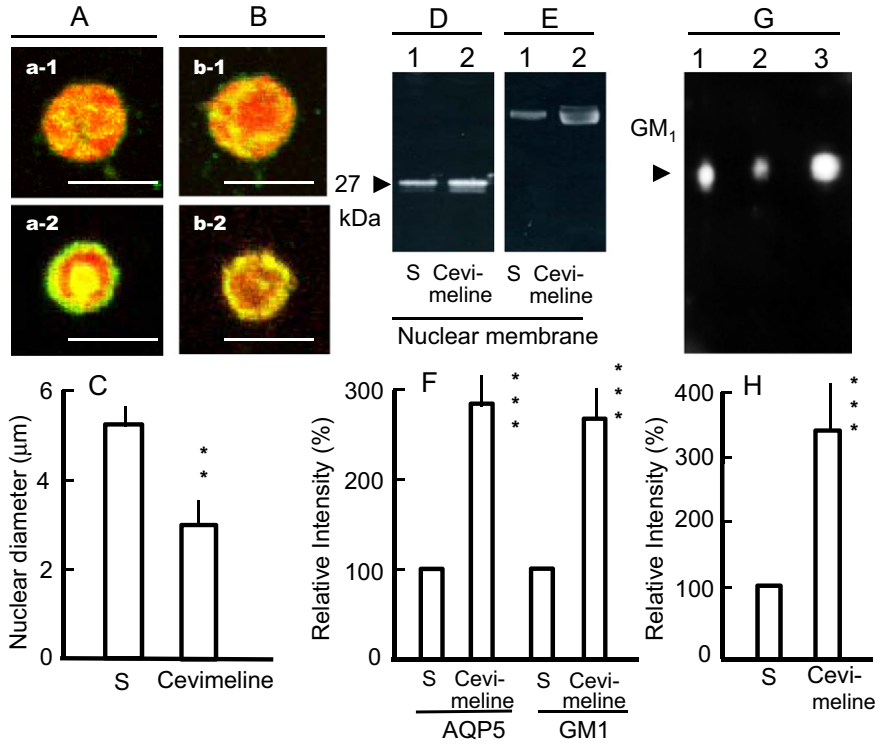

Fig. 5. AQP5 and GM1 distribution in isolated nuclear and subnuclear fractions. A–C) Isolated nuclei prepared from parotid glands at 3 min after cevimeline (a-2 and b-2) or saline (a-1 and b-1)-injection were incubated with anti-AQP5 (A) and anti-GM1 (B) antibodies. Nuclei were stained with propidium iodide. Bars: 5 μm. Diameter of stained nuclei from parotid glands 3 min after cevimeline or saline (S) (C) (n = 28). D–F) Nuclear membranes (D and E) were obtained from nuclei of parotid tissues treated with (lane 2) or without (lane 1) cevimeline. Each fraction was analyzed by immunoblot analysis with anti-AQP5 (D) and anti-GM1 (E) antibodies. Representative Western blot of AQP5 and GM1 was shown. Densitometric analysis is expressed in (H) as the relative intensity of chemiluminescene (n = 5). G–H) Gangliosides were extracted from isolated nuclei prepared from parotid glands at 3 min after cevimeline (lane 3) or saline (S) (lane 2) injection, and were then separated by TLC. The GM1 standard is shown in lane 1. Densitometric analysis is expressed in (H) as relative intensity of chemiluminescence (n = 3). ***$p < 0.001$ vs. value for saline-injected rats.

2.8. Immunoblot analysis in Western blotting and thin-layer chromatography (TLC)

Nuclear membrane, nucleoplasm, detergent-insoluble and -soluble domains, and F1-7 were subjected to sodium dodecyl sulfate-polyacrylamide gel electrophoresis on a 12.5% gel. Separated proteins were transferred to nitrocellulose membranes. Blots were probed with antibodies against AQP5, GM1 (1:1500), and Lamin B (1:1000), and were revealed by ECL detection [10]. Chemiluminescent blots were imaged with the ChemiDoc MP imager (Bio-Rad, Hercules, CA) and on film. Films were imaged with ChemiDoc MP using the white light conversion screen. Band Analysis tools of ImageLab software version 4.2 (Bio-Rad) were used to select and determine the background-subtracted density of bands. On the other hand, gangliosides were separated by TLC. GM1 purified standard (Sigma) was used as a positive control. Plates (aluminum-backed silica gel 60 plates-Merck) were soaked in a 1% solution of polyisobutyl methacrylate in hexane for 90 s, air dried, incubated in blocking solution (ECL) for 30 min, and were then treated with peroxidase-conjugated cholera-toxin B subunit (1:500; Sigma), as described previously [35,36]. Bands were revealed by ECL detection.

2.9. Immunoelectron microscopy

Tissue was prepared for electron microscopy by freeze substitution, as described previously [10]. Ultrathin Lowicryl HM20 sections were incubated overnight at 4 °C with anti-AQP5 antibodies, and were visualized with goat anti-rabbit IgG conjugated to 10-nm colloidal gold particles at a ratio of 1:50 IgG:gold particles (GAR.EM10; BioCell Research Laboratories, Cardiff, UK). Sections stained with uranyl acetate and lead citrate were examined with Philips CM100 or Philips Morgagni electron microscopes (Philips, Eindhoven, The Netherlands).

2.10. Statistical analysis

Data are presented as means ± standard error (SE), and were analyzed for statistical significance by Student's t-test or analysis of variance at all time points. P values of less than 0.05 were considered to be statistically significant.

3. Results

3.1. mAChR agonist-induced translocation of AQP5 to nuclear membrane, APM and lateral plasma membrane (LPM)

In order to maximize the immunostaining of AQP5 in parotid acinar cells, deeply pre-chilled ethanol was used for fixation of parotid tissues (Figs. 1–3, 5A and 5B), although formalin and methanol were used to investigate the localization of AQP5 in duct cells [10]. Under unstimulated conditions, AQP5 was present in three distinct compartments: some AQP5 was present in the APM, and large amounts of AQP5 were diffusely distributed in the apical plasmalemmal region and throughout the cytoplasm (Fig. 1A). This distribution is similar to that in mouse sweat glands [18]. Cevimeline was injected into the rat tail vein to visualize

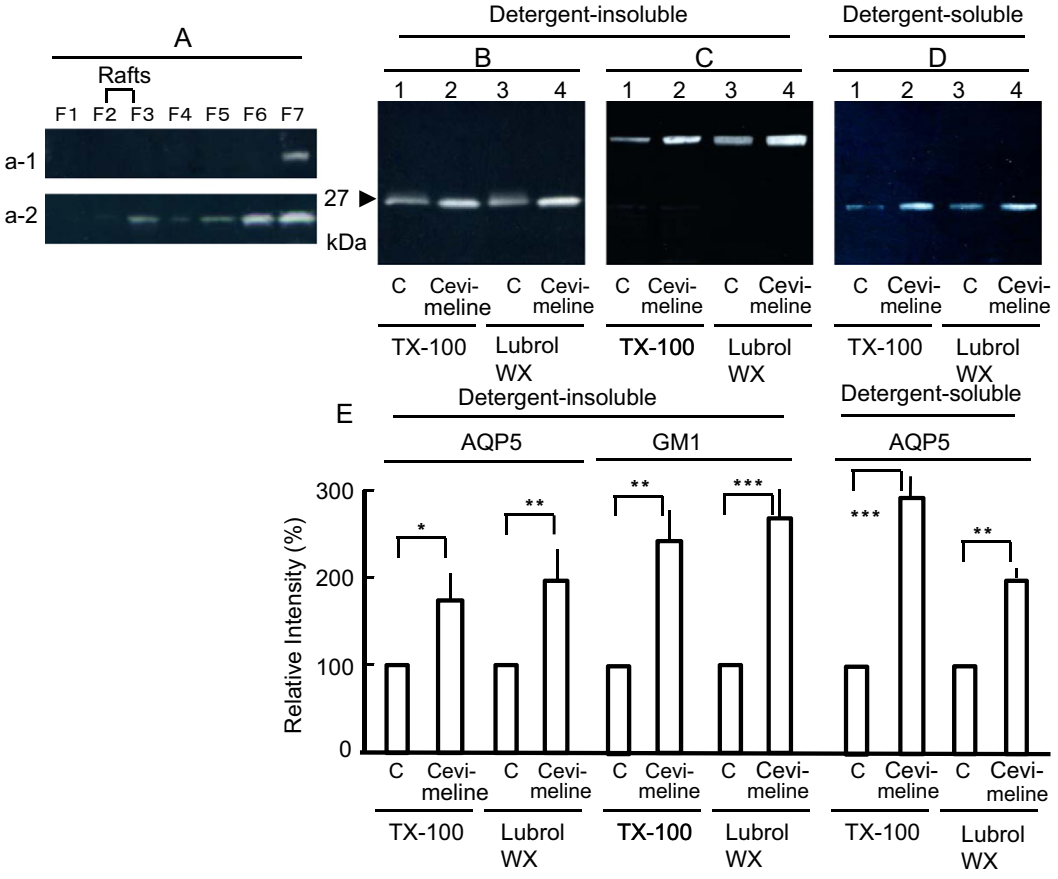

Fig. 6. Characterization of lipid rafts associated with AQP5 in nucleus. (A) Nuclei isolated from parotid glands at 3 min after cevimeline (a-2) or saline (a-1) injection were homogenized with TNE buffer containing 1% Triton X-100 (TX-100). Homogenates were added to 45% sucrose (W/V), which was overlaid with 45%, 35% and 5% sucrose. After centrifugation, fractions were collected from the top (F1) to the bottom (F6) of the gradients. The pellet was designated as F7. F1–F7 was subjected to immunoblot analysis with anti-AQP5. B–E) Nuclei were isolated from parotid tissues incubated with (lanes 2 and 4) or without (lanes 1 and 3, C) cevimeline for 3 min, and were then treated with TNE solution containing 1% TX-100 or 1% Lubrol WX. Detergent-insoluble (B and C) and -soluble (D) fractions were subjected to immunoblot analysis with anti-AQP5 (B and D) and anti-GM1 (C) antibodies. Densitometric analysis is expressed in (E) as relative intensity of chemiluminescence ($n = 5$). *$p < 0.05$, **$p < 0.01$, and ***$p < 0.01$ vs. value for control tissues.

the cellular distribution of AQP5 in acinar cells. After 1.5 to 3 min, localization of AQP5 in the nuclei was observed (Fig. 1B and 1C, arrows). After 6 to 10 min, AQP5 was located predominantly on the APM and LPM (Fig. 1D and 1E). After 60 min, AQP5 levels in the APM and the LPM were decreased and diffused into the cytoplasm (Fig. 1F).

3.2. Prevention of mAChR agonist-induced translocation of AQP5 by atropine

In order to investigate the effects of mAChR antagonists on subcellular distribution of AQP5, atropine was injected intraperitoneally. After 60 min, AQP5 was observed as small punctate staining throughout the cytoplasm, and there was less AQP5 in the APM and the LPM than under unstimulated conditions (Fig. 2D vs. 2A). Similarly to parotid tissues pre-incubated with atropine before exposure to mAChR agonist [7], atropine was pre-injected into rats in in vivo experiments (Fig. 2E and 2F), and 60 min later, cevimeline was injected intravenously. After 3 min, no AQP5 localization in the nucleus was observed (Fig. 2E vs. Fig. 2B and 2B′). After 10 min, AQP5 had not accumulated in the APM and LPM when compared with non-atropine treated sections (Fig. 2F vs. Fig. 2C). These results suggest that atropine prevented the cevimeline-induced increases in AQP5 in the nucleus, APM and LPM.

3.3. Translocation of AQP5 and lipid microdomains to nuclei and APM

We next investigated whether activation of mAChRs induces translocation of AQP5 together with lipid rafts containing flotillin-1 and GM1 to the nucleus. Under unstimulated conditions (Fig. 3a–f-1), AQP5 was co-localized with flotillin-1 in the cytoplasm and APM. Three minutes after cevimeline-injection (Fig. 3a–f-2), AQP5 and flotillin-1 were observed in the nucleus, APM, and LPM. Sixty minutes after cevimeline-injection (Fig. 3a–f-3), AQP5 disappeared from the nucleus. The localization of AQP5 in the APM was decreased and the cytosolic distribution of AQP5 was increased together with lipid rafts (Fig. 3f-3).

In order to confirm that cevimeline induces trafficking of AQP5 to nuclei, we analyzed acinar cells in sections from saline and cevimeline-treated rats by immunoelectron microscopy. Three minutes after administration of saline, AQP5 was mainly localized in intracellular compartments, but not in the nuclear membrane (Fig. 4B and 4C). Three minutes after administration of cevimeline, AQP5 was largely localized in the nuclear membrane (Fig. 4F).

Furthermore, to confirm that AQP5 is trafficked to the nucleus, nuclei were isolated from parotid glands. Under unstimulated conditions, some AQP5 (Fig. 5a-1) and GM1 (Fig. 5b-1) were found in isolated nuclei. Three minutes after cevimeline injection (Fig. 5a-2 and 5b-2), AQP5 localization in the nucleus was enhanced. Immunoblot analysis of AQP5 and GM1 in subnuclear fractions showed that, under unstimulated conditions, some AQP5 (Fig. 5D-1) and GM1 (Fig. 5E-1) were located in the nuclear membrane. Three minutes after cevimeline injection, AQP5 (Fig. 5D-2) and GM1 (Fig. 5E-2) levels increased in the nuclear membrane. In TLC experiments, GM1 was also increased in the nucleus 3 min after cevimeline injection (Fig. 5G-3). Thus, mAChR activation induced AQP5 trafficking to the nuclear membrane.

3.4. Characterization of lipid microdomains associated with AQP5 in nuclear membrane

In order to characterize the lipid microdomains in which AQP5 was located and trafficked to the nuclei, flotation experiments in sucrose density gradients (Fig. 6A) and differential detergent extraction of isolated nuclei were performed (Fig. 6B–D). In nuclei prepared from parotid glands 3 min after cevimeline injection, small increases in AQP5 were seen in F3 (light fraction), and large increases in AQP5 were seen in F6-7 (heavy fractions) (Fig. 6A, a-2).

Rat parotid tissues were incubated with or without cevimeline. Nuclei isolated from parotid glands treated with cevimeline for 3 min were homogenized with TNE solution containing 1% TX-100 and 1% Lubrol WX. Under unstimulated conditions, the major portion of AQP5 was present in the TX-100- or Lubrol WX-insoluble fraction (Fig. 6B and 6D). After incubation with cevimeline, AQP5 levels in the nucleus were increased in both the detergent-soluble (Fig. 6D) and -insoluble (Fig. 6B) fractions and GM1 was increased in the insoluble fraction (Fig. 6C).

Thus, the microdomains associated with AQP5 in the nuclear membrane were not present in the low density fraction in sucrose gradients. Upon activation of mAChRs, AQP5 localization was increased in both detergent-soluble and -insoluble microdomains of the nuclear membrane.

3.5. Function of AQP5 in nuclear membrane

Nuclei were isolated from rat parotid glands with or without cevimeline injection and were then stained with anti-AQP5 or anti-GM1 antibodies. To investigate the function of AQP5 in the nuclear membrane, we measured the diameter of parotid nuclei visualized with Alexa Fluour (Fig.5A and 5B). At 0 min, the diameter was 5.63 μm (Fig. 5C). However, at 3 min after cevimeline injection, the diameter had decreased to 3.44 μm (Fig. 5C). Nuclear shape was smooth and circular at 0, and was rough and irregular at 3 min (Fig. 5A and 5B).

Isolated nuclei were prepared from parotid tissues incubated with or without cevimeline for 3 min. The inner and outer nuclear membranes were prepared from isolated nuclei. Immunoblot analysis of AQP5 showed that, under unstimulated conditions, AQP5 was scarcely located in both nuclear membranes (Fig. 7, lanes 1 and 3). Three minutes after cevimeline injection, AQP5 levels increased in both the inner and outer nuclear membranes (Fig. 7, lanes 2 and 4). One third of AQP5 in the nuclear membrane was located in the inner nuclear membrane (Fig. 7B). Lamin B was used as a marker of inner nuclear membrane.

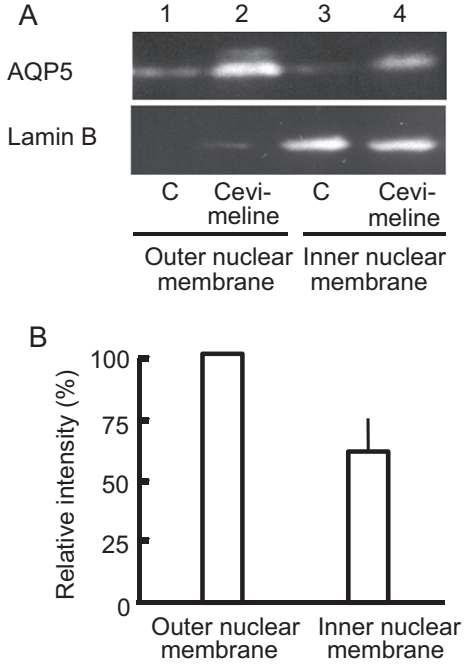

Fig. 7. AQP5 and Lamin B distribution in outer and inner nuclear membranes. Nuclear membranes were isolated from parotid tissues incubated with (lanes 2 and 4) or without (lanes 1 and 3) cevimeline for 3 min. Outer nuclear membranes (lanes 1 and 2) and inner nuclear membranes (lanes 3 and 4) were separated using 1% trisodium citric acid. Each membrane was subjected to immunoblot analysis with anti-AQP5 (A, upper panel) and anti-lamin B (A, lower panel) antibodies. Densitometric analysis of AQP5 in lanes 2 and 4 is expressed in (B) as relative intensity of chemiluminescence (n = 3).

Cevimeline induced contractions in nuclear size, thus suggesting that AQP5 plays a role in regulating water permeability in the nuclear membrane of rat parotid glands.

4. Discussion

The findings of the present study indicate that, under unstimulated conditions, AQP5 in parotid acinar cells is localized broadly in the APM and diffusely in the cytoplasm. The activation of mAChR induced AQP5 translocation to the nucleus and APM. Movement of AQP5 to the nucleus peaked from 90 s to 3 min after cevimeline injection. After 6 to 10 min, AQP5 was predominantly located in the APM and LPM. Sixty minutes after treatment, some AQP5 had moved back to the cytoplasm for reuse and the distribution resembled that of unstimulated glands. Prolonged atropine treatment (60 min) inhibited the cevimeline-induced translocation of AQP5 to the APM, LPM, and nucleus, thus suggesting that mAChR activation induced AQP5 translocation to the nucleus, LPM and APM in parotid glands.

Previously, we reported that AQP5 moves from the cytoplasm to the APM together with lipid rafts in parotid glands [10], and here, we investigated whether AQP5 was trafficked to the nucleus together with lipid rafts. Flotillin-1 and GM1 were used as markers for lipid rafts. Lipid rafts have two important characteristics: (i) resistance to detergent solubilization at low temperatures; and (ii) a low buoyant density [27–29]. In isolated nuclei, nuclear membranes prepared from parotid glands stimulated with cevimeline had larger amounts of AQP5, GM1, and flotillin-1, thus suggesting that AQP5, GM1, and flotillin-1 were trafficked to the nuclei. GM1 is present in the nucleus and is implicated in the regulation of nuclear signaling [37] and nuclear Ca^{2+} homeostasis [38]. Flotillins identified in nuclei-depleted detergent-resistant membrane shuttled between subcellular sites and the nucleus, and were not the result of contamination that occurred during extraction [39]. In addition, cevimeline induced increases in the amount of AQP5 in the TX-soluble and -insoluble fractions prepared from the nuclear membrane. However, small amounts of TX-insoluble AQP5 were seen at light density on sucrose density gradients. Cells produce sphingolipids and cholesterol in an anterograde secretory pathway, thereby maintaining low endoplasmic reticulum (ER) and nuclear envelope (NE) concentrations of these lipids [40,41]. Neither ER nor NE membranes contain sufficient cholesterol to support lipid-raft formation [42]. Taken together, these results indicate that upon stimulation by cevimeline, AQP5 moves to the nucleus together with microdomains containing flotillin-1 and GM1, but not cholesterol.

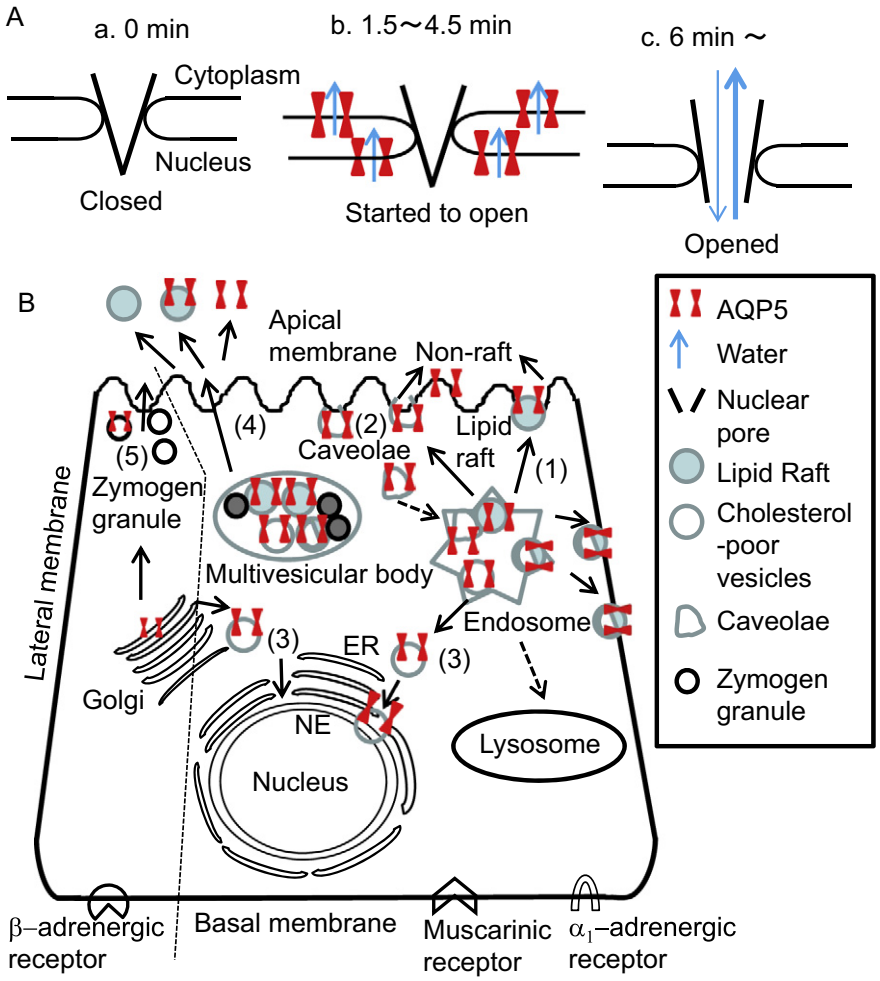

Fig. 8. Schematic diagram of AQP5 trafficking in rat parotid glands. A: Appearance and disappearance of AQP5 in nuclear membrane. At 0 min, small amounts of AQP5 were present in the nuclear membrane (a). At 1.5–4.5 min after cevimeline injection, the amount of AQP5 increased in the inner and outer nuclear membranes (b). At 6 min after cevimeline injection, AQP5 had disappeared from the nuclear membrane (c). B: Trafficking routes of AQP5 in rat parotid acinar cells. (1) Trafficking of AQP5 to the APM together with lipid rafts. (2) Internalizing of AQP5 together with caveolae. (3) Trafficking of AQP5 to nuclei together with cholesterol-poor and sphingolipid-rich microdomain. (4) AQP5 is released into saliva by exosomes. (5) Trafficking of AQP5 together with zymogen granules.

More recently, a wider range of detergents has been used to purify rafts, and different classes of rafts have been isolated [43]. Lipid rafts in the trans-Golgi network are soluble in TX-100 and insoluble in Lubrol [31], suggesting that the rafts have sphingolipid-rich membranes. In this experiment, detergent-resistant nuclear membrane microdomains that included AQP5 were insoluble in both TX-100 and Lubrol, suggesting that the microdomains were enriched in sphingolipids.

AQP5 is located in lipid rafts under control conditions in rat parotid glands. Upon activation of mAChR, AQP5 is trafficked to the APM together with lipid rafts, and is then translocated from lipid rafts (TX-insoluble fraction) to non-rafts (TX-soluble fraction) [10]. Caveolae are small, flask-shaped invaginations of the membrane [28] and form a subdomain of lipid rafts [44]. The characteristic protein components of caveolae are the caveolins [45]. Caveolin 1-deficient salivary gland acinar cells show reduced partitioning of AQP5 to raft microdomains [17]. Under prolonged atropine treatment conditions (60 min) or control conditions in rat parotid glands, lipid rafts containing AQP5 were distributed in at least two domains: the apical plasmalemmal microdomains including caveolae and lipid raft-derived vesicles in the cytosol. Allen et al. reported that trafficking by clathrin-independent lipid rafts may involve three distinct mechanisms: endocytosis mediated by caveolae; endocytosis mediated by planar lipid rafts; and/or lateral trafficking into or out of these microdomains [28].

In body fluids such as saliva, there are three main classes of extracellular vesicle: exosomes, microvesicles, and apoptotic bodies [46]. Exosomes form multivesicular bodies inside the cells and are secreted into body fluids when these bodies fuse with the plasma membrane [47–49] in tightly controlled Ca^{2+} -triggered reactions [15,16]. Exosomes are known to be rich in raft-lipids [16]. Parotid salivary exosomes contain AQP5 [50] and two different sizes of exosome prepared from whole saliva also contain AQP5 [14], suggesting that exosomes containing AQP5 are present in cytosolic multivesicular bodies in rat parotid glands. Associated with multivesicular bodies, cholesterol-rich small cytoplasmic vesicles and mostly cholesterol-negative vesicles are observed in B lymphocytes, and those enriched in cholesterol appeared to fuse with the cell surface to release exosomes [51]. Cholesterol displays a highly differential distribution in the various membrane domains of the endocytic pathway [52]. It is known that the nuclear envelope does not contain sufficient cholesterol to support lipid-raft formation [42], but it is unclear whether both cholesterol-rich cytoplasmic vesicles and cholesterol-poor cytoplasmic vesicles are present in parotid glands, as cholesterol-rich cytoplasmic vesicles translocate to the APM and cholesterol-poor cytoplasmic vesicles may translocate to nuclei in parotid acinar cells.

The primary function of AQPs located in the plasma membrane of the cell is to facilitate the passive transport of water across the membrane in response to osmotic gradients [53,54]. The findings of this study revealed that nuclear size decreases when AQP5 is trafficked to the nuclear membrane in parotid glands by the stimulation of mAChRs. AQP5 increased in both the inner and outer nuclear membranes, thus suggesting that AQP5 plays a role in the regulation of water transport across the nuclear membrane. Nuclear size is also sensitive to hyperosmolarity [55]. However, the nuclear pore complex (NPC) allows the free diffusion of water [56]. As shown in Fig. 8A, AQP5 in the nuclear membrane triggers the movement of water, inducing shrinkage of the nucleus. This small shrinkage opens NPC, allowing the free diffusion of water. While the nucleus decreases in size and the pores expand in the nuclear membrane, nucleocytoplasmic transport modulates gene transcription or translation of genetic information [57]. AQP5 located in the nuclear membrane may play a crucial role in the start of nuclear shrinkage and nuclear function.

Ion channels and receptors translocate from plasma membrane to nuclear membranes [58]. Tight crosstalk between receptors and ionic transporters in plasma membranes and those in nuclear membranes regulates cytosolic and nuclear ionic homeostasis. The regulation of cytosolic and nuclear water homeostasis may also depend on tight crosstalk between AQP5 in plasma membranes and that in nuclear membranes.

We show the trafficking routes of AQP5 in rat parotid glands in Fig. 8B. Five trafficking routes have been identified. Route 1 shows the movement of AQP5 to the APM together with lipid rafts [10]. Route 2 is the internalizing route for AQP5 together with caveolae [17]. Route 3 is the trafficking route for AQP5 to the nucleus together with cholesterol-poor and sphingolipid-rich microdomains (shown in this study). In route 4, AQP5 is released into saliva by exosomes [12,13]. Route 5 is the trafficking route for AQP5 together with zymogen granules [59,60]. In this study, we showed that AQP5 was trafficked from the non-apical region to the nuclear membrane and APM together with sphingolipid-rich vesicles in parotid acinar cells upon activation of mAChRs. In nuclei, AQP5 may be triggered to facilitate water transport across the nuclear membrane. Enhancement of $[Ca^{2+}]$i-induced trafficking of AQP5 is observed in eccrine sweat glands [18], submandibular glands [17,61] and human salivary gland cells [62]. The enhancement of c-APM-induced trafficking of AQP5 is seen in Brunner's glands [63,64] and lung epithelial cells [65]. In contrast, no trafficking of AQP5 is reported in the sublingual glands [66] and labial glands [67]. The newly reported functions of AQP5 include the facilitation of cell migration [68], the enhancement of microtubule organization and stability [69], and the transcription of disruptors of telomeric silencing and regulators of AQP2 [70]. We propose that AQP5 is trafficked to the nuclear membrane, as well as the APM, and this triggers water transport across the nuclear membrane upon activation of mAChR, leading to functional consequences for nucleocytoplasmic transport, gene transcription, and translation of genetic information.

Acknowledgments

This work was supported by a Grant-in-Aid for Scientific Research and for Knowledge Cluster Initiative from the Ministry of Education, Culture, Sports, Science and Technology of Japan (Grant number 23592738). Cevimeline was kindly provided by the Daiichi-Sankyo Pharmaceutical Co. (Tokyo, Japan). We are also grateful to the Iwadare Scholarship Foundation.

References

[1] G.B. Proctor, G.H. Carpenter, Regulation of salivary gland function by autonomic nerves, Auton. neurosci.: basic clin. 133 (2007) 3–18.
[2] I.S. Ambudkar, Ca(2+)signaling and regulation of fluid secretion in salivary gland acinar cells, Cell Calcium 55 (2014) 297–305.
[3] A. Rojek, J. Praetorius, J. Frokiaer, S. Nielsen, R.A. Fenton, A current view of the mammalian aquaglyceroporins, Annu. Rev. Physiol. 70 (2008) 301–327.
[4] K. Ishibashi, S. Kondo, S. Hara, Y. Morishita, The evolutionary aspects of aquaporin family, Regulatory, integrative and comparative physiologyAm. j. physiol. 300 (2011) R566–R576.
[5] S. Raina, G.M. Preston, W.B. Guggino, P. Agre, Molecular cloning and characterization of an aquaporin cDNA from salivary, lacrimal, and respiratory tissues, J. biol. chem. 270 (1995) 1908–1912.
[6] T. Ma, Y. Song, A. Gillespie, E.J. Carlson, C.J. Epstein, A.S. Verkman, Defective secretion of saliva in transgenic mice lacking aquaporin-5 water channels, J. biol. chem. 274 (1999) 20071–20074.
[7] Y. Ishikawa, T. Eguchi, M.T. Skowronski, H. Ishida, Acetylcholine acts on M3 muscarinic receptors and induces the translocation of aquaporin5 water channel via cytosolic Ca2+ elevation in rat parotid glands, Biochem. Biophys. Res. Commun. 245 (1998) 835–840.
[8] Y. Ishikawa, M.T. Skowronski, N. Inoue, H. Ishida, alpha(1)-adrenoceptor-induced trafficking of aquaporin-5 to the apical plasma membrane of rat parotid cells, Biochem. Biophys. Res. Commun. 265 (1999) 94–100.
[9] Y. Ishikawa, M.T. Skowronski, H. Ishida, Persistent increase in the amount of aquaporin-5 in the apical plasma membrane of rat parotid acinar cells induced by a muscarinic agonist SNI-2011, FEBS Lett. 477 (2000) 253–257.
[10] Y. Ishikawa, Z. Yuan, N. Inoue, M.T. Skowronski, Y. Nakae, M. Shono, G. Cho, M. Yasui, P. Agre, S. Nielsen, Identification of AQP5 in lipid rafts and its translocation to apical membranes by activation of M3 mAChRs in interlobular ducts of rat parotid gland, Am. J. Physiol. Cell Physiol. 289 (2005) C1303–C1311.
[11] Y. Ishikawa, G. Cho, Z. Yuan, N. Inoue, Y. Nakae, Aquaporin-5 water channel in lipid rafts of rat parotid glands, Biochim. Biophys. Acta 1758 (2006) 1053–1060.
[12] Y. Pan, F. Iwata, D. Wang, M. Muraguchi, K. Ooga, Y. Ohmoto, M. Takai, G. Cho, J. Kang, M. Shono, X.J. Li, K. Okamura, T. Mori, Y. Ishikawa, Identification of

aquaporin-5 and lipid rafts in human resting saliva and their release into cevimeline-stimulated saliva, Biochim. Biophys. Acta 1790 (2009) 49–56.
[13] M. Gonzalez-Begne, B. Lu, X. Han, F.K. Hagen, A.R. Hand, J.E. Melvin, J.R. Yates, Proteomic analysis of human parotid gland exosomes by multidimensional protein identification technology (MudPIT), J. Proteome Res. 8 (2009) 1304–1314.
[14] Y. Ogawa, Y. Miura, A. Harazono, M. Kanai-Azuma, Y. Akimoto, H. Kawakami, T. Yamaguchi, T. Toda, T. Endo, M. Tsubuki, R. Yanoshita, Proteomic analysis of two types of exosomes in human whole saliva, Biol. Pharm. Bull. 34 (2011) 13–23.
[15] A. Savina, M. Furlan, M. Vidal, M.I. Colombo, Exosome release is regulated by a calcium-dependent mechanism in K562 cells, J. Biol. Chem. 278 (2003) 20083–20090.
[16] M. Simons, G. Raposo, Exosomes—vesicular carriers for intercellular communication, Curr. Opin. Cell Biol. 21 (2009) 575–581.
[17] B. Pani, X. Liu, S. Bollimuntha, K.T. Cheng, I.R. Niesman, C. Zheng, V.R. Achen, H.H. Patel, I.S. Ambudkar, B.B. Singh, Impairment of TRPC1-STIM1 channel assembly and AQP5 translocation compromise agonist-stimulated fluid secretion in mice lacking caveolin1, J. Cell Sci. 126 (2013) 667–675.
[18] R. Inoue, E. Sohara, T. Rai, T. Satoh, H. Yokozeki, S. Sasaki, S. Uchida, Immunolocalization and translocation of aquaporin-5 water channel in sweat glands, J. Dermatol. Sci. 70 (2013) 26–33.
[19] S.P. Humphrey, R.T. Williamson, A review of saliva: normal composition, flow, and function, J. Prosthet. Dent. 85 (2001) 162–169.
[20] E. Roussa, Channels and transporters in salivary glands, Cell Tissue Res. 343 (2011) 263–287.
[21] K. Simons, E. Ikonen, Functional rafts in cell membranes, Nature 387 (1997) 569–572.
[22] D. Lingwood, K. Simons, Lipid rafts as a membrane-organizing principle, Science (New York, N.Y.) 327 (2010) 46–50.
[23] E. Rodriguez-Boulan, G. Kreitzer, A. Musch, Organization of vesicular trafficking in epithelia, Nat. Rev. Mol. Cell Biol. 6 (2005) 233–247.
[24] D. Delacour, R. Jacob, Apical protein transport, Cell. Mol. Life Sci.: CMLS 63 (2006) 2491–2505.
[25] X. Cao, M.A. Surma, K. Simons, Polarized sorting and trafficking in epithelial cells, Cell Res. 22 (2012) 793–805.
[26] A. Kusumi, K. Suzuki, Toward understanding the dynamics of membrane-raft-based molecular interactions, Biochim. Biophys. Acta 1746 (2005) 234–251.
[27] K. Simons, D. Toomre, Lipid rafts and signal transduction, Nat. Rev. Mol. Cell Biol. 1 (2000) 31–39.
[28] J.A. Allen, R.A. Halverson-Tamboli, M.M. Rasenick, Lipid raft microdomains and neurotransmitter signalling, Nat. Rev. Neurosci. 8 (2007) 128–140.
[29] M.G. Waugh, J.J. Hsuan, Preparation of membrane rafts, Methods Mol. Biol. (Clifton, N.J.) 462 (2009) 403–414.
[30] K. Roper, D. Corbeil, W.B. Huttner, Retention of prominin in microvilli reveals distinct cholesterol-based lipid micro-domains in the apical plasma membrane, Nat. Cell Biol. 2 (2000) 582–592.
[31] T.A. Slimane, G. Trugnan, I.S.C. Van, D. Hoekstra, Raft-mediated trafficking of apical resident proteins occurs in both direct and transcytotic pathways in polarized hepatic cells: role of distinct lipid microdomains, Mol. Biol. Cell 14 (2003) 611–624.
[32] H. Ishida, K. Ahmed, Studies on phosphoproteins of submandibular gland nuclei isolated from isoproterenol-treated rats, Exp. Cell Res. 78 (1973) 31–40.
[33] E. Albi, M. Micheli, M.P. Viola Magni, Phospholipids and nuclear RNA, Cell Biol. Int. 20 (1996) 407–412.
[34] J.S. Gilchrist, G.N. Pierce, Identification and purification of a calcium-binding protein in hepatic nuclear membranes, J. biol. chem. 268 (1993) 4291–4299.
[35] I. Tempera, B. Buchetti, E. Lococo, R. Gradini, A. Mastronardi, M.T. Mascellino, P. Sale, L. Mosca, M. d'Erme, L. Lenti, GD3 nuclear localization after apoptosis induction in HUT-78 cells, Biochem. Biophys. Res. Commun. 368 (2008) 495–500.
[36] M.C. Deregibus, V. Cantaluppi, R. Calogero, M. Lo Iacono, C. Tetta, L. Biancone, S. Bruno, B. Bussolati, G. Camussi, Endothelial progenitor cell derived microvesicles activate an angiogenic program in endothelial cells by a horizontal transfer of mRNA, Blood 110 (2007) 2440–2448.
[37] R.W. Ledeen, G. Wu, Sphingolipids of the nucleus and their role in nuclear signaling, Biochim. Biophys. Acta 1761 (2006) 588–598.
[38] R. Ledeen, G. Wu, GM1 in the nuclear envelope regulates nuclear calcium through association with a nuclear sodium–calcium exchanger, J. Neurochem. 103 (Suppl. 1) (2007) 126–134.
[39] R.M. Adam, W. Yang, D. Di Vizio, N.K. Mukhopadhyay, H. Steen, Rapid preparation of nuclei-depleted detergent-resistant membrane fractions suitable for proteomics analysis, BMC cell biol. 9 (2008) 30.
[40] S. Hoetzl, H. Sprong, G. van Meer, The way we view cellular (glyco)sphingolipids, J. Neurochem. 103 (Suppl. 1) (2007) 3–13.
[41] A. Czogalla, M. Grzybek, W. Jones, U. Coskun, Validity and applicability of membrane model systems for studying interactions of peripheral membrane proteins with lipids, Biochim. Biophys. Acta 1841 (2014) 1049–1059.
[42] I.W. Mattaj, Sorting out the nuclear envelope from the endoplasmic reticulum, Nat. Rev. Mol. Cell Biol. 5 (2004) 65–69.
[43] L.H. Chamberlain, Detergents as tools for the purification and classification of lipid rafts, FEBS Lett. 559 (2004) 1–5.
[44] P. Lajoie, I.R. Nabi, Lipid rafts, caveolae, and their endocytosis, Int. Rev. Cell Mol. Biol. 282 (2010) 135–163.
[45] R.G. Parton, M.A. del Pozo, Caveolae as plasma membrane sensors, protectors and organizers, Nat. Rev. Mol. Cell Biol. 14 (2013) 98–112.
[46] A.V. Vlassov, S. Magdaleno, R. Setterquist, R. Conrad, Exosomes: current knowledge of their composition, biological functions, and diagnostic and therapeutic potentials, Biochim. Biophys. Acta 1820 (2012) 940–948.
[47] K. Denzer, M.J. Kleijmeer, H.F. Heijnen, W. Stoorvogel, H.J. Geuze, Exosome: from internal vesicle of the multivesicular body to intercellular signaling device, J. Cell Sci. 113 (Pt 19) (2000) 3365–3374.
[48] A. Lakkaraju, E. Rodriguez-Boulan, Itinerant exosomes: emerging roles in cell and tissue polarity, Trends Cell Biol. 18 (2008) 199–209.
[49] J. Kowal, M. Tkach, C. Thery, Biogenesis and secretion of exosomes, Curr. Opin. Cell Biol. 29C (2014) 116–125.
[50] W. Yan, R. Apweiler, B.M. Balgley, P. Boontheung, J.L. Bundy, B.J. Cargile, S. Cole, X. Fang, M. Gonzalez-Begne, T.J. Griffin, F. Hagen, S. Hu, L.E. Wolinsky, C.S. Lee, D. Malamud, J.E. Melvin, R. Menon, M. Mueller, R. Qiao, N.L. Rhodus, J.R. Sevinsky, D. States, J.L. Stephenson, S. Than, J.R. Yates, W. Yu, H. Xie, Y. Xie, G.S. Omenn, J.A. Loo, D.T. Wong, Systematic comparison of the human saliva and plasma proteomes, Proteomics Clin. Appl. 3 (2009) 116–134.
[51] W. Mobius, Y. Ohno-Iwashita, E.G. van Donselaar, V.M. Oorschot, Y. Shimada, T. Fujimoto, H.F. Heijnen, H.J. Geuze, J.W. Slot, Immunoelectron microscopic localization of cholesterol using biotinylated and non-cytolytic perfringolysin O, J. Histochem. Cytochem.:Offic.J. Histochem. Soc. 50 (2002) 43–55.
[52] W. Mobius, E. van Donselaar, Y. Ohno-Iwashita, Y. Shimada, H.F. Heijnen, J.W. Slot, H.J. Geuze, Recycling compartments and the internal vesicles of multivesicular bodies harbor most of the cholesterol found in the endocytic pathway, Traffic (Copenhagen, Denmark), 42003. 222–231.
[53] S. Nielsen, T.H. Kwon, J. Frokiaer, P. Agre, Regulation and dysregulation of aquaporins in water balance disorders, J. Intern. Med. 261 (2007) 53–64.
[54] R.E. Day, P. Kitchen, D.S. Owen, C. Bland, L. Marshall, A.C. Conner, R.M. Bill, M.T. Conner, Human aquaporins: regulators of transcellular water flow, Biochim. Biophys. Acta 1840 (2014) 1492–1506.
[55] J.D. Finan, K.J. Chalut, A. Wax, F. Guilak, Nonlinear osmotic properties of the cell nucleus, Ann. Biomed. Eng. 37 (2009) 477–491.
[56] S.R. Wente, M.P. Rout, The nuclear pore complex and nuclear transport, Cold Spring Harb. Perspect. Biol. 2 (2010) a000562.
[57] J.D. Finan, H.A. Leddy, F. Guilak, Osmotic stress alters chromatin condensation and nucleocytoplasmic transport, Biochem. Biophys. Res. Commun. 408 (2011) 230–235.
[58] G. Bkaily, L. Avedanian, J. Al-Khoury, L. Ahmarani, C. Perreault, D. Jacques, Receptors and ionic transporters in nuclear membranes: new targets for therapeutical pharmacological interventions, Can. J. Physiol. Pharmacol. 90 (2012) 953–965.
[59] T. Susa, N. Sawai, T. Aoki, A. Iizuka-Kogo, H. Kogo, A. Negishi, S. Yokoo, K. Takata, T. Matsuzaki, Effects of repeated administration of pilocarpine and isoproterenol on aquaporin-5 expression in rat salivary glands, Acta histochem. cytochem. 46 (2013) 187–197.
[60] M. Matsuki, S. Hashimoto, M. Shimono, M. Murakami, J. Fujita-Yoshigaki, S. Furuyama, H. Sugiya, Involvement of aquaporin-5 water channel in osmoregulation in parotid secretory granules, J. Membr. Biol. 203 (2005) 119–126.
[61] J.H. Kim, S.H. Park, Y.W. Moon, S. Hwang, D. Kim, S.H. Jo, S.B. Oh, J.S. Kim, J.W. Jahng, J.H. Lee, S.J. Lee, S.Y. Choi, K. Park, Histamine H1 receptor induces cytosolic calcium increase and aquaporin translocation in human salivary gland cells, J. Pharmacol. Exp. Ther. 330 (2009) 403–412.
[62] J. Tada, T. Sawa, N. Yamanaka, M. Shono, T. Akamatsu, K. Tsumura, M.N. Parvin, N. Kanamori, K. Hosoi, Involvement of vesicle-cytoskeleton interaction in AQP5 trafficking in AQP5-gene-transfected HSG cells, Biochem. Biophys. Res. Commun. 266 (1999) 443–447.
[63] M.N. Parvin, S. Kurabuchi, K. Murdiastuti, C. Yao, C. Kosugi-Tanaka, T. Akamatsu, N. Kanamori, K. Hosoi, Subcellular redistribution of AQP5 by vasoactive intestinal polypeptide in the Brunner's gland of the rat duodenum, Am. J. Physiol. Gastrointest. Liver Physiol. 288 (2005) G1283–G1291.
[64] A.M. Collaco, R.L. Jakab, N.E. Hoekstra, K.A. Mitchell, A. Brooks, N.A. Ameen, Regulated traffic of anion transporters in mammalian Brunner's glands: a role for water and fluid transport, Am. J. Physiol. Gastrointest. Liver Physiol. 305 (2013) G258–G275.
[65] V. Sidhaye, J.D. Hoffert, L.S. King, cAMP has distinct acute and chronic effects on aquaporin-5 in lung epithelial cells, J. biol. chem. 280 (2005) 3590–3596.
[66] W. Masuda, E. Jimi, CD38/ADP-ribosyl cyclase in the rat sublingual gland: subcellular localization under resting and saliva-secreting conditions, Arch. Biochem. Biophys. 513 (2011) 131–139.
[67] V. Gresz, A. Horvath, I. Gera, S. Nielsen, T. Zelles, Immunolocalization of AQP5 in resting and stimulated normal labial glands and in Sjogren's syndrome, Oral Dis. 21 (2015) 114–120.
[68] A.S. Verkman, More than just water channels: unexpected cellular roles of aquaporins, J. Cell Sci. 118 (2005) 3225–3232.
[69] V.K. Sidhaye, E. Chau, V. Srivastava, S. Sirimalle, C. Balabhadrapatruni, N.R. Aggarwal, F.R. D'Alessio, D.N. Robinson, L.S. King, A novel role for aquaporin-5 in enhancing microtubule organization and stability, PLoS One 7 (2012) e38717.
[70] H. Wu, L. Chen, X. Zhang, Q. Zhou, J.M. Li, S. Berger, Z. Borok, B. Zhou, Z. Xiao, H. Yin, M. Liu, Y. Wang, J. Jin, M.R. Blackburn, Y. Xia, W. Zhang, Aqp5 is a new transcriptional target of Dot1a and a regulator of Aqp2, PLoS One 8 (2013) e53342.